Original Article

Investigation of Different Components of Parallel-Hole Collimator Response to Different Radioisotope Energies Used in Nuclear Medicine Imaging

Mahsa Noori-Asl, Sara Jeddi-Dashghapou
Department of Physics, Faculty of Science, University of Mohaghegh Ardabili, Ardabil, Iran

Abstract

Introduction: The quality of images obtained from the nuclear medicine imaging systems depends on different factors. One of the most important of these factors is the geometrical and physical characteristics of collimator used for imaging with a given radioisotope. **Aims and Objectives:** The aim of this study is to investigate the contribution of different components of collimator response for determining the most suitable parallel-hole collimator for the different radioisotope energies used in nuclear medicine imaging. **Materials and Methods:** In this study, the SIMIND Monte Carlo simulation program is used to determine the contribution of geometrical, penetrating and scattered response components of four hexagonal parallel-hole collimators including low-energy high-resolution (LEHR), low-energy general-purpose (LEGP), medium-energy general-purpose (MEGP), and high-energy general-purpose (HEGP) collimators, for 12 different energies used in nuclear medicine imaging. **Results:** According to the simulation results, the use of both the LEHR and LEGP collimators leads to a geometrical component above 60% for energies between 69 and 171 keV. On the other hand, for energies between 185 and 245 keV, the MEGP collimator and for energy of 364 keV, the HEGP collimator gives the geometrical components above 70% and 60%, respectively, while for energy of 511 keV, the geometrical response of all four collimators is below 20%. **Conclusion:** The results of this study show that for two low-energy single-photopeak radioisotopes, Tc-99m and I-123, the LEHR and LEGP collimators, and for high-energy single-photopeak radioisotope, I-131, the HEGP collimator are most suitable collimators. For dual-photopeak In-111 radioisotope and triple-photopeak Ga-67 radioisotope, the MEGP and HEGP collimators and for triple-photopeak Tl-201 radioisotopes, the LEHR and LEGP collimators are proposed as most suitable collimators.

Keywords: Collimator response, Monte Carlo simulation, nuclear medicine imaging

Received on: 12-01-2022 **Review completed on:** 21-02-2022 **Accepted on:** 02-05-2022 **Published on:** 08-11-2022

Introduction

The quality of images obtained from the nuclear medicine imaging systems is affected by different factors such as the physical properties of detector[1,2] and collimator,[3-5] image reconstruction algorithms,[6,7] photon attenuation[8-10] and scattering,[11-13] and patient motion.[14-16] The use of a suitable collimator when imaging with a given radioisotope is an essential factor to produce the high quality images. The collimator is usually a thick lead sheet containing a large number of fine holes that provides accurate information about the initial emission location of the photons by restricting the incident photon acceptance angle.[17] The combination of three parameters, including hole diameter, septa width, and collimator thickness determine the collimator response to the gamma rays emitted in different directions. Furthermore, the used collimator determines the geometric field of view, and affects the spatial resolution and the sensitivity of the imaging system, significantly. The four main types of collimators are used in nuclear medicine imaging, including the parallel-hole, diverging-hole, converging-hole, and pin-hole collimators. Each of these collimators may be used depending on the region being

Access this article online

Quick Response Code:

Website: www.jmp.org.in

DOI: 10.4103/jmp.jmp_3_22

Address for correspondence: Dr. Mahsa Noori-Asl, Department of Physics, Faculty of Science, University of Mohaghegh Ardabili, Ardabil, Iran.
E-mail: nooriasl.mahsa@gmail.com

How to cite this article: Noori-Asl M, Jeddi-Dashghapou S. Investigation of different components of parallel-hole collimator response to different radioisotope energies used in nuclear medicine imaging. J Med Phys 2022;47:294-300.

imaged. Among these, parallel-hole collimators are commonly used in clinical imaging.[18]

In an ideal parallel-hole collimator, only those photons that travel parallel to the collimator holes can pass through the holes and reach the detector surface.[4] Therefore, an ideal collimator should be large enough in thickness and small enough in hole diameter to remove all the photons with other directions. On the other hand, to increase the sensitivity of the imaging system, thinner collimators with larger hole diameters are required, which lead to reduce the spatial resolution of the imaging system due to the increased photon acceptance angle. Therefore, to avoid excessive loss of sensitivity and spatial resolution, it is necessary to choose an optimal collimator thickness and diameter between these two limits. In general, the response of collimators used in the imaging systems consists of three separate components: geometrical, penetrating, and scattered components[19] [Figure 1]. The geometrical component is related to the photons that pass directly through the holes of collimator. The penetrating component is the part of the collimator response in which, the photons pass through the septa material without interaction. Finally, the scattered component corresponds to the scattered photons in the collimator septa that reach to the detector surface. The contributions of these components change with the photon energy, the collimator design, and the source-collimator distance.[20] Obviously, a suitable collimator for radioisotope imaging should have the highest contribution of geometrical component and the lowest contributions of penetrating and scattered components.

In this study, Monte Carlo simulation was used to investigate the contributions of geometrical, penetrating, and scattered response components of low-energy high-resolution (LEHR), low-energy general-purpose (LEGP), medium-energy general-purpose (MEGP), and high-energy general-purpose (HEGP) parallel-hole collimators by imaging a point source.

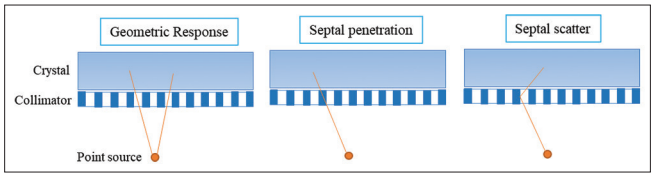

Figure 1: Illustration of three main components of the parallel-hole collimator response

Materials and Methods

In this study, the SIMIND Monte Carlo program (version 6.2) was used to simulate the single-photon emission computed tomography (SPECT) imaging system with four different hexagonal parallel-hole collimators including LEHR, LEGP, MEGP, and HEGP collimators. The geometrical characteristics of these collimators are given in Table 1 and Figure 2. A point source in air was used to investigate the different components of collimator response. The reason for using the point source without attenuating medium was to remove the complexities associated with the interactions of emitted photons before reaching the imaging system. This study was performed on 12 different energies: 11 different radioisotope energies used in SPECT and 511 keV energy of annihilation photons used in positron emission tomography. The characteristics of six widely used radioisotopes in SPECT imaging are given in Table 2. Furthermore, the energy spectra of these radioisotopes are shown in Figure 3.

Results

The results obtained from the simulation of four studied parallel-hole collimators for 12 different energies are given in Table 3 and Figures 4-7.

Figure 4 shows the results obtained from the simulation of LEHR collimator. From this figure, we can see that the geometrical component includes more than 60% of the collimator response for energies between 75 keV and 185 keV. For energies between 245 keV and 511 keV, this component

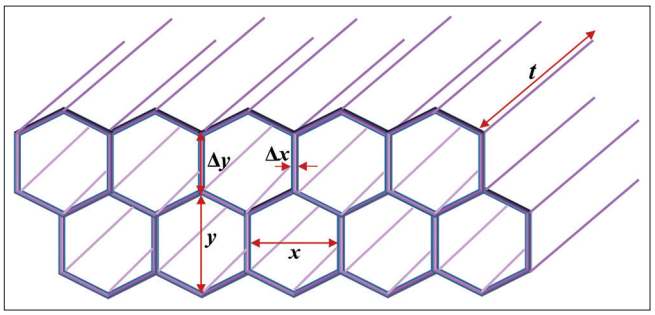

Figure 2: Illustration of different parameters of the hexagonal parallel-hole collimator

Table 1: The geometrical characteristics of four hexagonal parallel-hole collimators (cm)

Collimator type	Hole size (x)	Hole size (y)	Distance between two holes in x-direction (Δx)	Distance between two holes in y-direction (Δy)	Collimator thickness (t)
LEHR	0.15	0.173	0.02	0.121	3.5
LEGP	0.19	0.219	0.02	0.144	3.5
MEGP	0.3	0.346	0.105	0.355	5.8
HEGP	0.4	0.462	0.18	0.543	6.6

LEHR: Low-energy high-resolution, LEGP: Low-energy general-purpose, MEGP: Medium-energy general-purpose, HEGP: High-energy general-purpose

decreases to below 7% and the penetrating component increases from 26.12% to 80.70%. On the other hand, the scattered component shows an increasing and decreasing behavior, so that the maximum value of this component occurs at the energy of 245 keV (30.70%). The effect of decreasing the geometrical component and increasing the penetrating and scattered components at energies higher than 245 keV appears as a star artifact around the point source image.

Table 2: The characteristics of common radioisotopes used in SPECT imaging

Radionuclide	$t_{1/2}$ (h)	Emission type	Energy (keV)
^{99m}Tc	6.02	γ, IT	140
^{201}Tl	73	γ, EC	68 (X-ray), 135, 167
^{123}I	13	γ, EC	159
^{67}Ga	78.1	γ, EC	93, 185, 300
^{111}In	67.2	Auger e$^-$, EC	171, 245
^{131}I	192.5	γ, IT	364

From Figure 5, a similar behavior is observed when using the LEGP collimator. For energies up to 159 keV, the geometrical components do not show significant differences with the results of the LEHR collimator. For the energies of 167, 171, and 185 keV, the contribution of this component decreases more than 10% compared to that for the LEHR collimator, so that at energy of 185 keV, the value of this component reduces to below 50%. The remarkable point is that the values of geometrical and penetrating components at the energy of 185 keV are comparable to each other, this is clear from the point source image as well. As can be seen, unlike the LEHR collimator, there is a star artifact around the point source image at the energy of 185 keV.

From Table 1, due to the increase in hole diameter, distance between holes and collimator thickness of the MEGP and

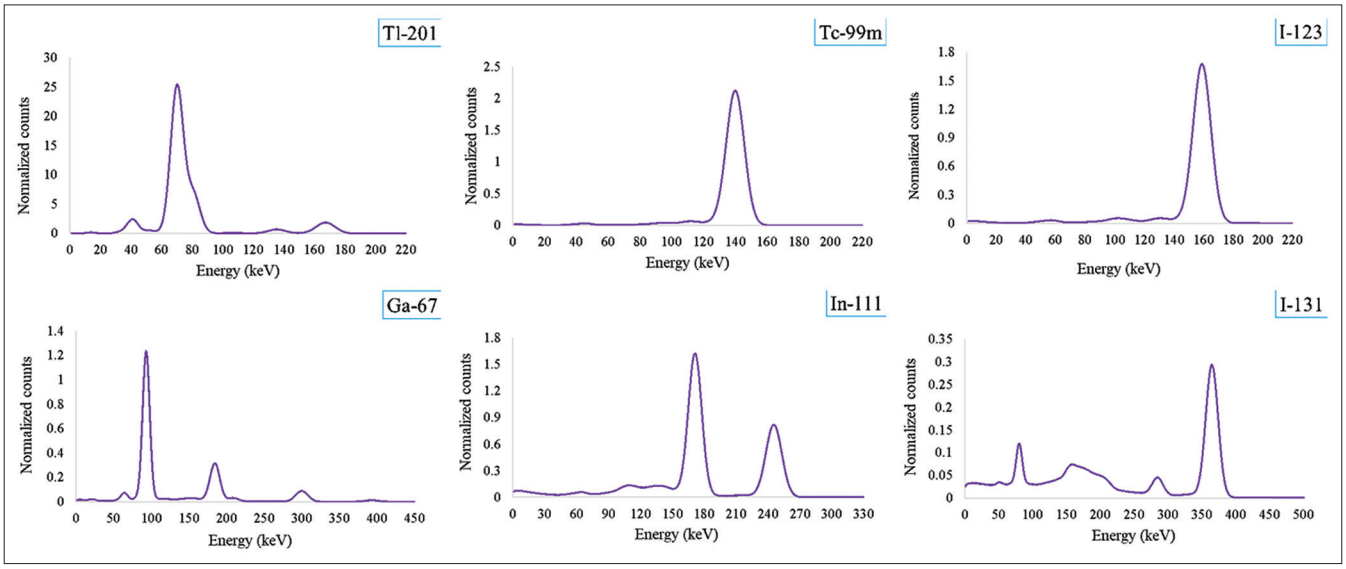

Figure 3: Energy spectra from simulation of a point source in air for six widely used radioisotopes in SPECT imaging. SPECT: Single photon emission computed tomography

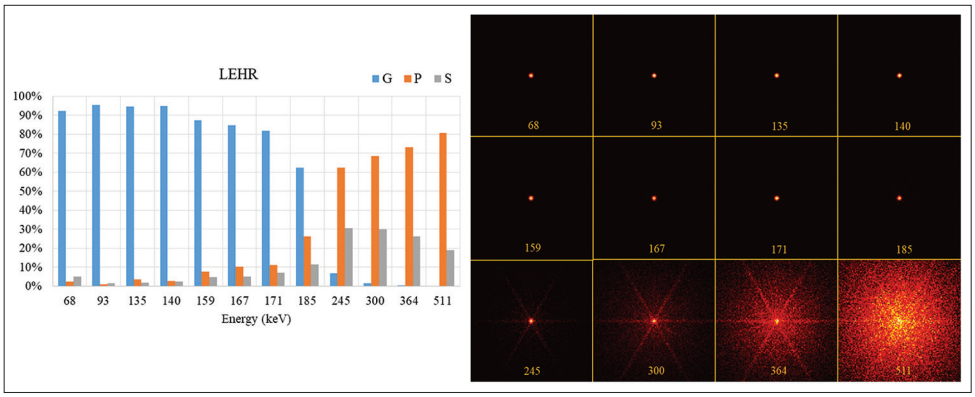

Figure 4: Diagrams of geometrical (g), penetrating (p) and scattered (s) components of the LEHR collimator response for 12 different energies together with corresponding images. LEHR: Low-energy high-resolution

Table 3: The geometrical, penetrating and scattered components of the response of four collimators for 12 different energies

Energy (keV)	LEHR (%)			LEGP (%)			MEGP (%)			HEGP (%)		
	geometrical	Penetrating	Scattered	geometrical	Penetrating	Scattered	geometrical	Penetrating	Scattered	geometrical	Penetrating	Scattered
68	92.42	2.50	5.08	91.67	2.67	5.66	93.98	1.14	4.88	93.71	0.94	5.35
93	95.54	1.16	1.59	94.51	1.80	1.96	95.96	0.98	1.44	96.68	0.52	1.72
135	94.59	3.51	1.90	94.27	3.27	2.46	96.91	1.44	1.65	96.85	1.05	2.10
140	94.81	2.63	2.56	92.82	4.49	2.69	96.41	2.24	1.35	97.40	1.24	1.36
159	87.49	7.80	4.71	83.97	11.10	4.93	95.81	2.06	2.13	96.36	1.47	2.17
167	84.74	10.28	4.99	73.40	17.84	8.76	94.37	4.05	1.59	95.97	1.69	2.33
171	81.72	11.13	7.15	68.35	22.71	8.94	94.20	3.46	2.34	95.54	2.38	2.08
185	62.33	26.12	11.54	44.70	39.85	15.45	93.35	4.25	2.40	96.68	2.09	1.24
245	6.86	62.44	30.70	4.78	67.64	27.58	86.46	8.85	4.69	91.47	4.87	3.65
300	1.60	68.45	29.94	1.27	73.04	25.69	72.54	16.06	11.41	83.19	11.80	5.01
364	0.54	73.14	26.33	0.57	76.74	22.69	33.58	36.32	30.09	66.28	20.53	13.19
511	0.21	80.70	19.09	0.25	83.53	16.22	3.75	57.12	39.12	13.19	46.32	40.19

LEHR: Low-energy high-resolution, LEGP: Low-energy general-purpose, MEGP: Medium-energy general-purpose, HEGP: High-energy general-purpose

HEGP collimators compared to two low-energy collimators, we expect an increase in the contribution of the geometrical component and a decrease in the contribution of the penetrating component for these collimators. This is clear from the data in Table 3 as well as Figures 6 and 7.

In the case of the MEGP collimator, a significant increase in the contribution of geometrical component and a decrease in the penetrating component are observed, especially for the three energies of 185, 245, and 300 keV, which lead to the elimination of star artifact from the point source image of these three energies [Figure 6]. However, due to the presence of large contributions of penetrating and scattered components at higher energies, 364 keV and 511 keV, the point source images of these energies are not clear yet, but as can be seen, this blurring is significantly lower than that for the LEGP collimator. Furthermore, unlike the LEHR and LEGP collimators, the scattered component shows a continuous increasing trend.

In the case of the HEGP collimator, the obtained results do not show considerable differences with those for the MEGP collimator for energies below 300 keV. However, in higher energies, due to further increase in the contribution of geometrical component and the decrease in the penetrating component, especially at the energy of 364 keV, the point source image for this energy is much clearer than that for the MEGP collimator. For the energy of 511 keV, although there is still a star artifact, but its value is significantly lower than that for the MEGP collimator [Figure 7].

Figure 8 shows the linear profiles from an arbitrary slice of the point source reconstructed images for three energies, low energy 159 keV, medium energy 245 keV, and high energy 364 keV, using four studied collimators. It should be noted that although according to the diagrams in Figures 4-7, the percentage of geometrical components of the MEGP and HEGP collimators for all energies is higher than those for the LEHR and LEGP collimators, but, due to the high volume of the collimator material, the number of photons reaching the detector surface, and therefore, the total recorded counts are much less than those for two low-energy collimators.

According to the obtained results, it is possible to determine the optimal collimator for the single-photopeak radioisotopes (Tc-99m, I-123, and I-131) from the photopeak energies. However, for the multi-photopeak radioisotopes (In-111, Ga-67, and Tl-201), it is necessary to consider the collective effect of photopeaks by using the actual energy spectra of these radioisotopes.

In order to determine the components of collimator response in the case of the multi-photopeak radioisotopes, in the first step, it is necessary to determine the suitable energy windows required for imaging, based on the photopeak energies of these radioisotopes. In this study, we use two energy windows for dual-photopeak In-111 radioisotope (two 20% energy windows centered at 171 keV and 245 keV), and

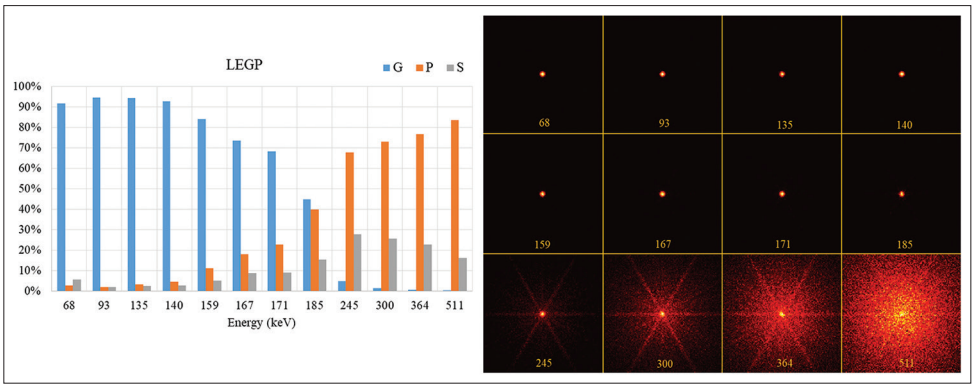

Figure 5: Diagrams of geometrical (g), penetrating (p) and scattered (s) components of the LEGP collimator response for 12 different energies together with corresponding images. LEGP: Low-energy general-purpose

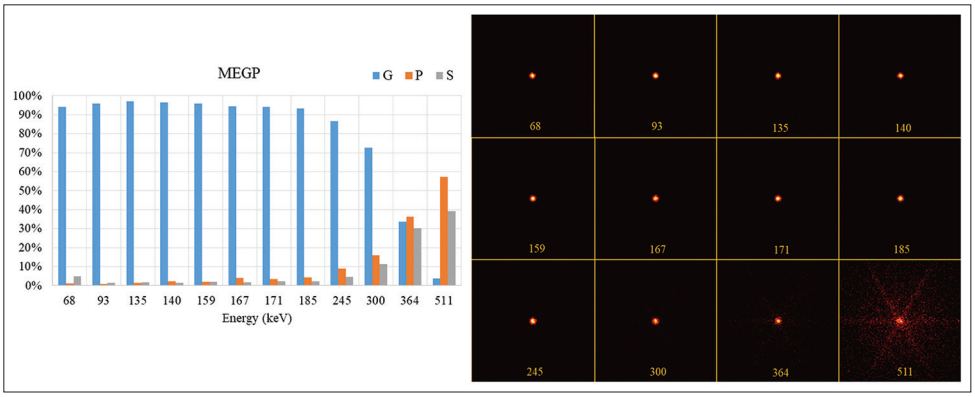

Figure 6: Diagrams of geometrical (g), penetrating (p) and scattered (s) components of the MEGP collimator response for 12 different energies together with corresponding images. MEGP: Medium-energy general-purpose

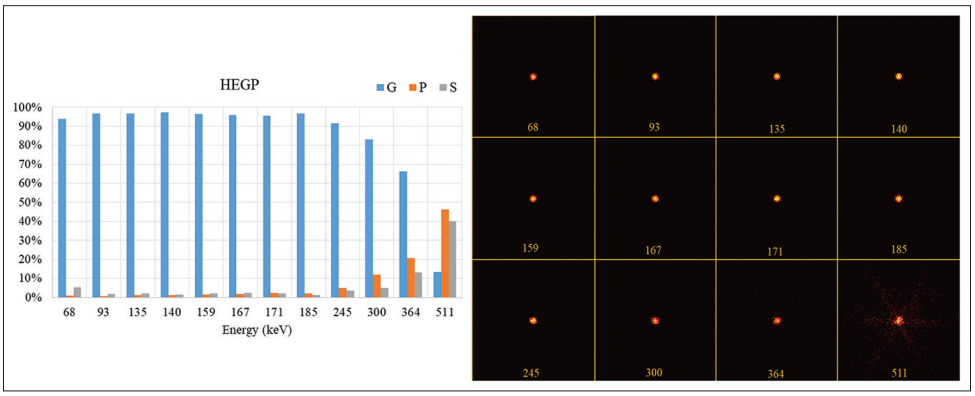

Figure 7: Diagrams of geometrical (g), penetrating (p) and scattered (s) components of the HEGP collimator response for 12 different energies together with corresponding images. HEGP: High-energy general-purpose

three energy windows for triple-photopeak radioisotopes, Ga-67 (30%, 20% and 15% windows centered at 93, 185, and 300 keV, respectively) and Tl-201 (30%, 20%, and 20% windows centered at 68, 135, and 167 keV, respectively). In the next step, from the total counts and the percentages of geometrical, penetrating and scattered components obtained for each windows, we calculate the total contribution of each these components for the LEGP, MEGP, and HEGP collimators. Figures 9 and 10 show the results obtained from these simulations. Due to the similar behavior of low-energy collimators, only the LEGP collimator response is investigated here.

From Figure 9, we can see that the use of LEGP collimator when imaging with In-111, results in a very low geometrical component (about 11.4%) and a very large contribution of penetrating component (more than 60%). This appears as a star artifact in the point source image. On the other hand, by

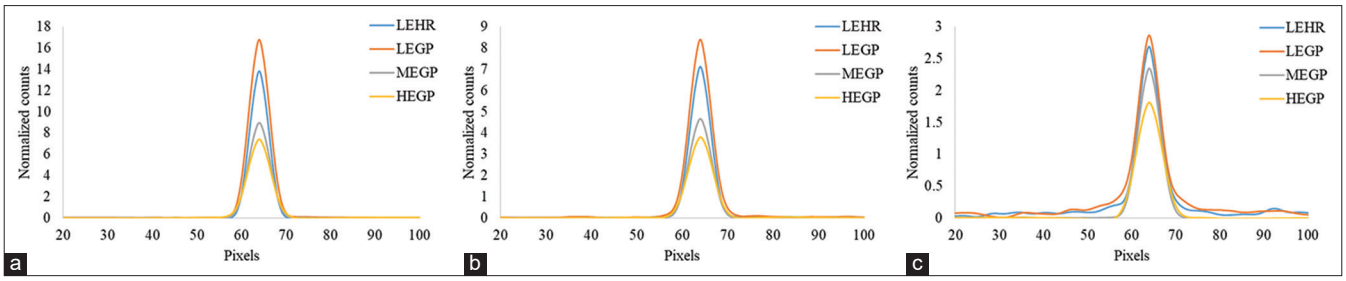

Figure 8: Profiles from an arbitrary slice of the point source reconstructed images for three energies of (a) 159 keV, (b) 245 keV and (c) 364 keV by using LEHR, LEGP, MEGP, HEGP collimators. LEHR: Low-energy high-resolution, LEGP: Low-energy general-purpose, MEGP: Medium-energy general-purpose, HEGP: High-energy general-purpose

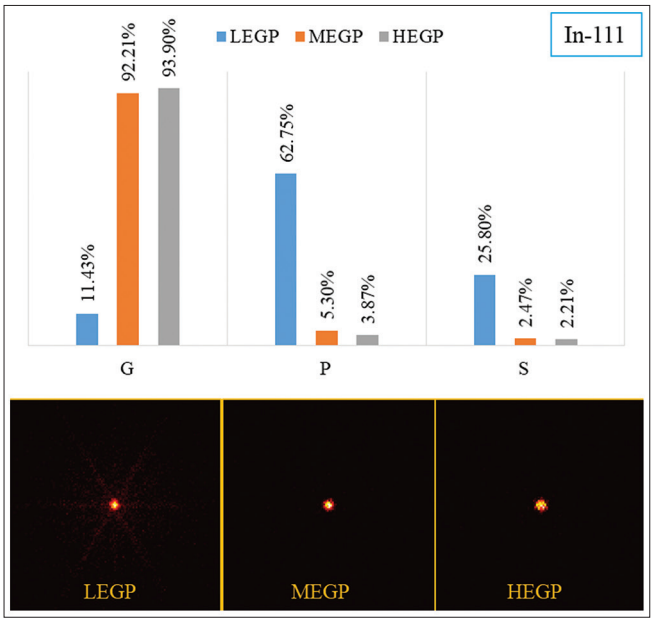

Figure 9: Diagrams of geometrical (g), penetrating (p) and scattered (s) components of the response of the LEGP, MEGP and HEGP collimators for dual-photopeak Indium-111 radioisotope. LEGP: Low-energy general-purpose, MEGP: Medium-energy general-purpose, HEGP: High-energy general-purpose

using the MEGP and HEGP collimators, the contribution of the geometrical component increases to more than 90% and the contributions of undesirable penetrating and scattered components decrease to below 6% and 3%, respectively. The clear images of the point source confirm these results. The results from the simulations of triple-photopeak radioisotopes, Tl-201 and Ga-67, are shown in Figure 10. From this figure, the results for Ga-67 are approximately similar to those for dual-photopeak In-111 radioisotope. The reason for this result is that three photopeaks of Ga-67 are placed in different three energy ranges (93, 185, and 300 keV in low, medium, and high energy ranges, respectively). In the case of Tl-201 with three low-energy photopeaks, the use of all three collimators gives approximately same results.

Discussion and Conclusion

According to the simulation results, when using the low-energy single-photopeak radioisotopes, Tc-99m (140 keV) and I-123 (159 keV), the best choices are the LEHR and LEGP collimators. From Table 1, all physical characteristics of these two collimators are the same except the diameter of holes. Due to this difference, the LEGP collimator is used when producing the images with more sensitivity is desired, and the LEHR collimator is chosen to produce the higher contrast images. For the high-energy single-photopeak radioisotope, I-131 (364 keV), only in the case of the HEGP collimator, the contribution of the geometrical component is approximately twice the sum of contributions of the other two components (66.28% vs. 33.72%). Therefore, among the four studied collimators, the HEGP collimator is the only suitable option for imaging with this radioisotope.

In the case of In-111 radioisotope with two main photopeaks (171 keV and 245 keV), both the MEGP and HEGP collimators give desirable results. However, it should be noted that although the HEGP collimator shows a slightly higher contribution of the geometrical component compared to the MEGP collimator, but, due to the increase in the volume of the collimator material and the increase in the diameter of holes, the number of counts, and also, the image contrast decreases when using the HEGP collimator. Therefore, due to more sensitivity and higher spatial resolution, the MEGP collimator is a more suitable option when using this radioisotope.

On the other hand, for imaging with triple-photopeak Ga-67 radioisotope with three photopeaks in different energy ranges (93, 185, and 300 keV in low, medium, and high energy ranges, respectively), similar to dual-photopeak In-111 radioisotope, both the MEGP and HEGP collimators can be used. In the case of second triple-photopeak radioisotope, thallium-201, all three collimators give almost similar results for the contributions of three components. However, for more sensitivity and higher image contrast, the LEHR and LEGP collimators are proposed as a most suitable collimators for imaging with this radioisotope.

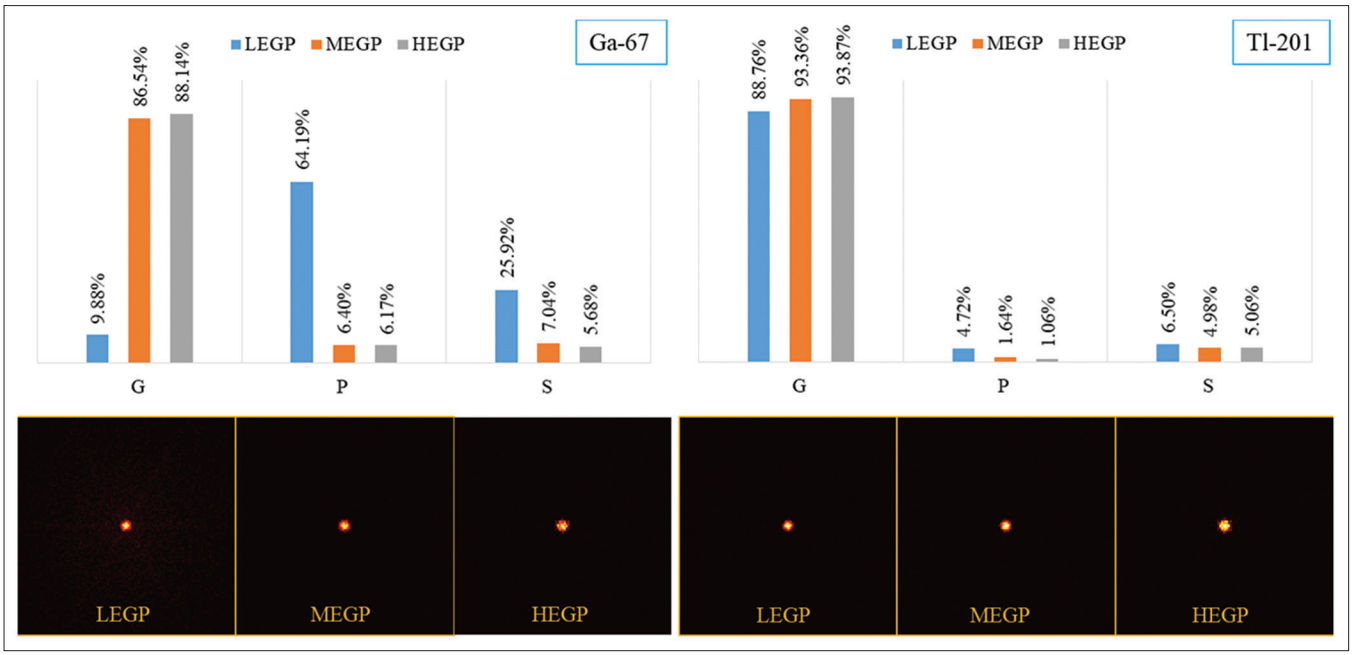

Figure 10: Diagrams of geometrical (G), penetrating (P) and scattered (S) components of the response of the LEGP, MEGP and HEGP collimators for triple-photopeak radioisotopes, Gallium-67 (left) and Thallium-201 (right). LEGP: Low-energy general-purpose, MEGP: Medium-energy general-purpose, HEGP: High-energy general-purpose

Finally, from the simulation results, none of the four studied collimators give an acceptable result for the energy of 511 keV. Therefore, it is necessary to design a suitable collimator for high-energy radioisotope imaging.

Financial support and sponsorship

Nil.

Conflicts of interest

There are no conflicts of interest.

References

1. Abbaspour S, Mahmoudian B, Islamian JP. Cadmium telluride semiconductor detector for improved spatial and energy resolution radioisotopic imaging. World J Nucl Med 2017;16:101-7.
2. Khoshakhlagh M, Islamian JP, Abedi M, Mahmoudian B, Mardanshahi AR. A study on determination of an optimized detector for single photon emission computed tomography. World J Nucl Med 2016;15:12-7.
3. Pandey AK, Sharma SK, Karunanithi S, Kumar P, Bal C, Kumar R. Characterization of parallel-hole collimator using Monte Carlo simulation. Indian J Nucl Med 2015;30:128-34.
4. Razavi SH, Kalantari F, Bagheri M, Namiranian N, Nafisi-Moghadam R, Mardanshahi A, *et al*. Characterization of low, medium and high energy collimators for common isotopes in nuclear medicine: A Monte Carlo study. Iran J Nucl Med 2017;25:100-4.
5. Azarm A, Islamian JP, Mahmoudian B, Gharepapagh E. The effect of parallel-hole collimator material on image and functional parameters in SPECT imaging: A SIMIND Monte Carlo study. World J Nucl Med 2015;14:160-4.
6. Bruyant PP. Analytic and iterative reconstruction algorithms in SPECT. J Nucl Med 2002;43:1343-58.
7. Zakavi SR, Zonoozi A, Kakhki VD, Hajizadeh M, Momennezhad M, Ariana K. Image reconstruction using filtered backprojection and iterative method: Effect on motion artifacts in myocardial perfusion SPECT. J Nucl Med Technol 2006;34:220-3.
8. Naji M, Zakavi SR, Hajizadeh M, Momennezhad M. Evaluation of attenuation correction process in cardiac SPECT images. Iran J Nucl Med 2008;16:1-7.
9. Raza H, Jadoon LK, Mushtaq S, Jabeen A, Maqbool M, Ul Ain M, *et al*. Comparison of non-attenuation corrected and attenuation corrected myocardial perfusion SPECT. Egypt J Radiol Nucl Med 2016;47:783-92.
10. Zhang Q, Zhang D, Mok GS. Comparison of different attenuation correction methods for dual gating myocardial perfusion SPECT/CT. IEEE Trans Radiat Plasma Med Sci 2019;3:565-71.
11. Asl MN, Sadremomtaz A, Bitarafan-Rajabi A. Evaluation of six scatter correction methods based on spectral analysis in (99m) Tc SPECT imaging using SIMIND Monte Carlo simulation. J Med Phys 2013;38:189-97.
12. Noori-Asl M, Sadremomtaz A, Bitarafan-Rajabi A. Evaluation of three scatter correction methods based on estimation of photopeak scatter spectrum in SPECT imaging: A simulation study. Phys Med 2014;30:947-53.
13. Noori-Asl M. Assessment of four scatter correction methods in In-111 SPECT imaging: A simulation study. J Med Phys 2020;45:107-15.
14. Leslie WD, Dupont JO, McDonald D, Peterdy AE. Comparison of motion correction algorithms for cardiac SPECT. J Nucl Med 1997;38:785-90.
15. O'Connor MK, Kanal KM, Gebhard MW, Rossman PJ. Comparison of four motion correction techniques in SPECT imaging of the heart: A cardiac phantom study. J Nucl Med 1998;39:2027-34.
16. Salehi N, Fatemizadeh E, Farahani MH, Akbarzadeh A, Farzanefar S, Ay MR. Cardiac contraction motion correction in gated myocardial perfusion SPECT projection domain. Front Biomed Technol 2015;2:206-13.
17. Kijewski MF. Positron emission tomography (PET) and single-photon emission computed tomography (SPECT) physics. In: Newton HB, editor. Handbook of Neuro-Oncology Neuroimaging. Ch 32, 2nd ed. San Diego, CA, USA: Academic Press; 2016. pp. 353-8.
18. Van Audenhaege K, Van Holen R, Vandenberghe S, Vanhove C, Metzler SD, Moore SC. Review of SPECT collimator selection, optimization, and fabrication for clinical and preclinical imaging. Med Phys 2015;42:4796-813.
19. Zaidi H. Quantitative Analysis in Nuclear Medicine Imaging. New York: Springer; 2006.
20. Sadremomtaz A, Telikani Z. Evaluation of the performance of parallel-hole collimator for high resolution small animal SPECT: A Monte Carlo study. Iran J Nucl Med 2016;24:136-43.